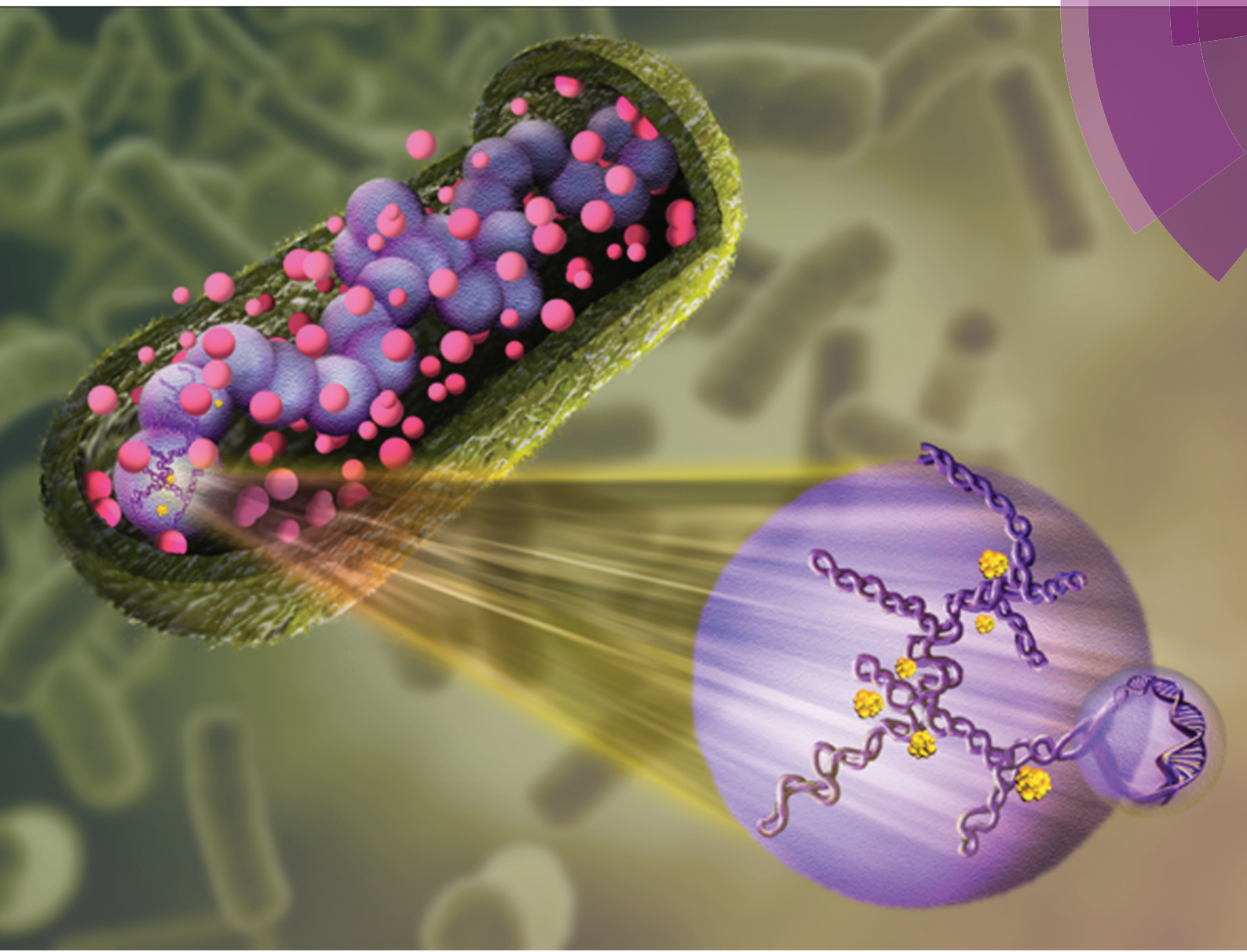


Soft Matter

www.softmatter.org



ISSN 1744-683X



PAPER

Juin Kim, Chanil Jeon, Hawoong Jeong, Youngkyun Jung and
Bae-Yeon Ha

A polymer in a crowded and confined space: effects of crowder size
and polydispersity



Cite this: *Soft Matter*, 2015, **11**, 1877

A polymer in a crowded and confined space: effects of crowder size and poly-dispersity

Juin Kim,^{a,b} Chanil Jeon,^b Hawoong Jeong,^{*acd} Youngkyun Jung^{*e} and Bae-Yeon Ha^{*b}

DNA compaction in a bacterial cell is in part carried out by entropic (depletion) forces induced by "free" proteins or crowding particles in the cytoplasm. Indeed, recent *in vitro* experiments highlight these effects by showing that they alone can condense the *E. coli* chromosome to its *in vivo* size. Using molecular dynamics simulations and a theoretical approach, we study how a flexible chain molecule can be compacted by crowding particles with variable sizes in a (cell-like) cylindrical space. Our results show that with smaller crowding agents the compaction occurs at a lower volume fraction but at a larger concentration such that doubling their size is equivalent to increasing their concentration fourfold. Similarly, the effect of polydispersity can be correctly mimicked by adjusting the size of crowders in a homogeneous system. Under different conditions, however, crowding particles can induce chain adsorption onto the cylinder wall, stretching the chain, which would otherwise remain condensed.

Received 2nd October 2014
 Accepted 8th December 2014

DOI: 10.1039/c4sm02198c
www.rsc.org/softmatter

1 Introduction

The bacterial chromosome, macroscopically long along its backbone (~ 2 mm for *E. coli*), occupies an intracellular space of micron size only, known as the nucleoid.^{1,2} How can this be accomplished in concert with other cellular or subcellular processes in the cell such as chromosome segregation and cell division, possibly without introducing much redundancy? Cells are crowded with biomolecules such as proteins and RNA^{1–7} (for an 'artist impression' of crowdedness,⁴ see ref. 3 and 4). For instance, a typical *E. coli* cell contains $\sim 10^6$ cytoplasmic proteins, occupying a large ($\sim 20\%$) fraction of the cell volume.^{2,4,6} While the complete picture of chromosome compaction is still elusive, it has often been attributed to three distinct factors: nucleoid-associated proteins, DNA super-coiling, and entropic (depletion) forces induced by "free" proteins and other crowding agents available in the cell^{1,2,8–12} (see ref. 13–15 for depletion forces in more general contexts). The first two factors are, however, thought to be insufficient for the full compaction of a chromosome.^{10,11} On the other hand, recent single molecule experiments suggest that depletion forces alone can condense the *E. coli* chromosomes to their *in*

vivo size,¹⁶ highlighting the favorable effects of molecular crowding once labelled as 'obvious but under-appreciated'.⁴

A few biological uncertainties make it challenging to interpret the compaction experiments.¹⁶ First, the *E. coli* chromosome is structurally heterogeneous. This might be responsible for the observed coexistence between condensed and extended phases, which would otherwise be interpreted as a signature of abrupt transitions. Indeed, chain collapse appears to be initiated preferentially at some region in the chromosome during the repeated compaction-decompaction cycle (see Movie S5 in ref. 16). Consideration of a simpler system, *i.e.*, a polymer in a confined and crowded space, will be beneficial for clarifying the role of molecular crowding in condensing a chain molecule and thus possibly for advancing our understanding of chromosome compaction in a cell.

Here, we carry out molecular dynamics simulations of a self-avoiding polymer in a crowded and confined space, as a coarse-grained model of the bacterial chromosome that captures only the essential features of chain molecules in a crowded space: chain connectivity as well as the excluded volume of chain segments and crowders. We treat monomers and crowders on an equal footing (both explicitly). Here, a large degree of coarse-graining is inevitable for various reasons. First, the physical properties of chromosomes have only begun to be revealed (see ref. 16–18 for recent progress). Also, the explicit treatment of crowders interacting with a long polymer is computationally demanding. Indeed, the degree/nature of coarse-graining in a physical approach to a biological system should reflect the desired level of abstraction *vs.* specificity. As evidenced later, this much simplified model leads to a few experimentally-testable predictions, which we believe will be useful for clarifying

^aDepartment of Physics, Korea Advanced Institute of Science and Technology, Daejeon 305-701, Korea. E-mail: hjeong@kaist.edu

^bDepartment of Physics and Astronomy, University of Waterloo, Waterloo, Ontario, N2L 3G1, Canada. E-mail: byha@uwaterloo.ca

^cInstitute for the BioCentury, Korea Advanced Institute of Science and Technology, Daejeon 305-701, Korea

^dAPCTP, Pohang, Gyeongbuk 790-784, Korea

^eNational Institute of Supercomputing and Networking, Korea Institute of Science and Technology Information, Daejeon 305-806, Korea. E-mail: yjung@kisti.re.kr

the role of depletion forces in organizing chromosomes in a confined cell-like space.

In our work, each monomer represents a structural unit consisting of supercoiled DNA strands and DNA-bound proteins,^{1,16,19,20} as illustrated in Fig. 1 (see below for details). We complement our simulation, limited to a relatively-short chain, with a free-energy approach, which is valid in the long chain-limit. Our simulation results suggest that crowding effects are strong enough to condense the chain in a cylindrical space, similarly to what was observed for the *E. coli* chromosome.¹⁶ They also indicate that the compaction is steep but continuous. While this is consistent with our theoretical prediction, its seeming contradiction with the phase coexistence observed for the *E. coli* chromosomes¹⁶ can be attributed to the structural heterogeneity and other biological details. Indeed, recent studies indicate an abrupt compaction of DNA molecules by dextran in a cylindrical tube but a continuous compaction in a slit-like or unconfined space.^{21,22} (Dextran is a polymeric crowder.) Furthermore, flexible chains in an unconfined space were shown to undergo a smooth compaction by crowding effects,²³ similarly to what our results suggest. Accordingly, a continuous compaction appears to be a general feature of flexible chains whether confined or free. What remains to be clarified further is to what extent the nature of chain compaction is controlled by the interplay between confinement and chain stiffness/heterogeneity (see ref. 22 and below for relevant discussions).

With smaller crowding particles, the compaction occurs at a smaller volume fraction but at a larger concentration. This is a

general feature of crowding effects and remains relevant for DNA compaction by dextran.^{21,22} Our results show a clear picture of the interplay between crowder sizes and densities: doubling their size is equivalent to increasing their concentration four-fold. We also consider chain compaction in a mixture of small and large crowders. We find that poly(bi)-dispersity will not change chain compaction qualitatively; its effect can be adequately mimicked by adjusting the size of crowders in a corresponding homogeneous system.

Under different conditions, however, the depletion force between monomers and the cylindrical wall is strong enough to promote chain adsorption onto the cylinder wall. As a result, the chain stretches, which would otherwise remain condensed, leading to a reentrant-like transition.

Molecular crowding influences other processes such as molecular reaction and diffusion, bimolecular aggregation, translation, and cell growth.^{4,5,24–26} For instance, this effect contributes to genome organization by enhancing DNA looping.²⁴ On the other hand, molecular crowding is shown to limit translation and cell growth by slowing down the diffusion of tRNA complexes.²⁵ In a recent study, it is considered as a physical origin of the glassy behavior of the bacterial cytoplasm.²⁶

Despite its relevance in a variety of contexts,^{4,5,24,25} our focus is on clarifying the nature/role of molecular crowding in the large-scale organization of chain molecules (e.g., bacterial chromosomes). After outlining the simulation procedure in Section 2, we present our numerical and theoretical results in Section 3.

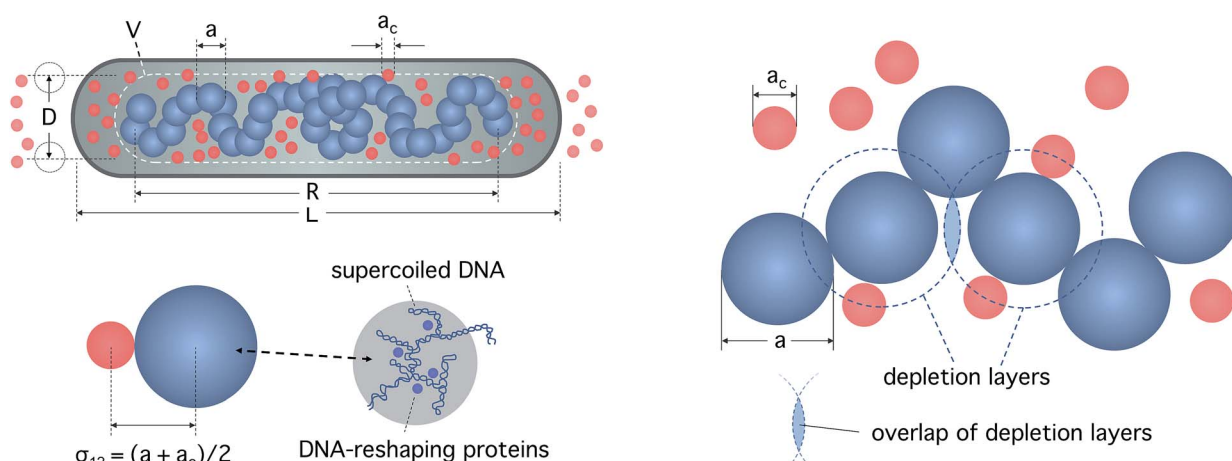


Fig. 1 (Left) Minimalist model of the nucleoid: beads on a string in a crowded and confined space. Note that in our simulation the cylinder is much longer than it appears in this illustration; it is about three times the equilibrium length of the chain R_0 in the absence of crowders. The entire system, excluding the chain trapped in the volume V , is then periodically reproduced. Thus it better mimics the micro-channel experimental setting¹⁶ than *E. coli* cells. The chain consists of N monomers or beads of diameter a each; the crowding particles are hard spheres of diameter a_c each. The cylinder diameter D is defined as the maximum distance between the centers of two monomers aligned vertically, as shown in the top left corner. The closest center-to-center distance between two spheres (monomers or crowders) sets naturally the parameter σ_{ij} that describes their interaction range (one of them is shown in the bottom panel). Each monomer in our work may represent a structural unit in the bacterial chromosome.¹⁶ (Right) Depletion forces induced by crowding agents: by overlapping the depletion layers (dashed circles) around two neighbouring monomers, the system increases the entropy of crowders. The resulting entropic force is known as depletion force. If V_{overlap} is the volume of the overlapped (shaded) region, it can be expressed as a function of the center-to-center distance of the two monomers denoted as r : $V_{\text{overlap}}(r) = \frac{\pi}{6}(a + a_c - r)^2(a + a_c + r/2)$;¹⁵ it reaches its maximum at $r = a$, given by $V_{\text{overlap}}(r = a) = \frac{\pi}{6}a_c^2(3a/2 + a_c) \equiv \Delta V_{\text{max}}$. Let Π_c be the osmotic pressure of crowders in a monomer-free region, then the depletion force between two monomers is given by $f_{\text{dep}} \approx \Pi_c \times \partial V_{\text{overlap}}/\partial r$. Of particular interest is the maximum free energy gain of two monomers when brought in contact: $\Delta F_{\text{max}} \approx \rho_c \Delta V_{\text{max}} \sim \rho_c a_c^2(3a/2 + a_c) \sim \phi(1 + 3a/2a_c)$.

2 Molecular dynamics simulations

In our simulations, we have to specify interactions between various pairs, monomer–monomer, monomer–crowder, crowder–crowder pairs, along with interactions of monomers or crowders with the cylindrical wall. In our simulations, the cylindrical wall is formed by imaginary spherical particles, which are of the same kind as monomers. Let r be the center-to-center distance between two particles. They interact with each other through the fully-repulsive Weeks–Chandler–Anderson (WCA) potential,²⁷ given by

$$U_{\text{WCA}}(r) = \begin{cases} 4\epsilon_{ij} \left[\left(\frac{\sigma_{ij}}{r} \right)^{12} - \left(\frac{\sigma_{ij}}{r} \right)^6 + \frac{1}{4} \right] & \text{for } r < 2^{1/6}\sigma_{ij} \\ 0 & \text{otherwise} \end{cases}. \quad (1)$$

Here the subscripts $i, j = 1, 2, 3$ are used to refer to monomers, crowders, and wall-forming particles, respectively: $\sigma_1 = \sigma_{11} = \sigma = a$ (monomer size), $\sigma_2 = \sigma_{22} = a_c$ (crowder size), and $\sigma_{12} = \sigma_{21} = (\sigma_1 + \sigma_2)/2, \dots$, and $\sigma_{33} = \sigma_1$. Finally, ϵ_{ij} measures the strength of U_{WCA} for various interaction pairs.

Chain connectivity between two consecutive monomers is ensured by the finitely-extensible non-linear elastic (FENE) potential described by^{28,29}

$$U_{\text{FENE}}(r) = -\frac{1}{2}kr_0^2 \ln \left[1 - \left(\frac{r}{r_0} \right)^2 \right], \quad (2)$$

where $k = 30.0\epsilon_{11}/\sigma$ and $r_0 = 1.5\sigma$.

Our simulation mimics the experimental setting¹⁶ better than the nucleoid in that the cylinder has open ends. This allows us to examine how crowders condense the chain from R_0 , the equilibrium length of the confined chain in the absence of crowders, which is much longer than the nucleoid length. In our simulation, the length of the cylinder L is three times R_0 ; periodic boundary conditions are then imposed on crowders at the cylinder ends.

For a similar reason, we initially set $\epsilon_{13} = \epsilon_{31}$ to 5.0 (for the interaction between the cylinder wall and monomers), so as to prevent the monomer adhesion to the cylinder wall, while setting all other ϵ_{ij} to 1.0 (in units of $\epsilon_{11} \equiv \epsilon$). In micro-channels, chromosome adhesion to the channel wall was chemically discouraged.¹⁶ A similar physical picture was assumed in the concentric-shell model of the nucleoid, where the chromosome is mostly confined inside the inner cylinder.^{30,31} Finally we also examined how the choice of $\epsilon_{13} = \epsilon_{31}$ is implicated in chain compaction or chain adsorption. To this end, we varied it from 1.0 to 10.0.

The equation of motion is integrated using the velocity-Verlet algorithm with a time step $0.002\tau_0$, where $\tau_0 = \sigma\sqrt{m/\epsilon}$ (m is the bead mass). We keep the system at a constant temperature given by $T = 1.0\epsilon/k_B$ via a Langevin thermostat with a damping constant $\gamma = 0.1\tau_0^{-1}$ (see ref. 32 and 33 and references therein).† Here and below, k_B is the Boltzmann constant

† The value of γ is not so crucial in determining equilibrium quantities, even though it is expected to influence short time-scale dynamics (see for instance ref. 36).

and T the temperature. In our actual simulations, the simulation package LAMMPS was used.³⁴

Here we chose the farthermost distance as the chain size³⁵ and measured it every 1000 integration steps after the chain equilibrated. (The farthermost distance suffers less from effects of finite-chain sizes³⁵ and is more free from numerical artifacts.) The ensemble average $\langle \dots \rangle$ was taken over more than 20 independent simulations and over about 5×10^7 integration steps for each simulation. The ensemble-average of the chain size was obtained as a function of the volume fraction of crowding agents.

For our simulation, we chose the number of monomers $N = 80$ and a number of crowding particles up to 100 000, depending on the volume fraction of crowding particles ϕ_c . The sizes (diameters) of crowding particles were $a_c = 0.2, 0.3, 0.4, 0.6, 0.8$ (in units of $\sigma = a$).

3 Results

3.1 Chain compaction: crowder sizes and poly(bi)-dispersity

First, we have examined how crowding particles condense a confined chain from its equilibrium length $R_0 \sim Na(D/a)^{-2/3}$ (in the absence of crowding particles).^{37,38} In all of our simulations, the chain consists of $N = 80$ monomers, immersed in the “sea” of crowders, as illustrated in Fig. 1; recall that our simulation setting resembles the experimental setting¹⁶ (see Section 2).

Fig. 2 displays our results for chain compaction for various parameter choices, for a mono-disperse (a) and bi-disperse case (b); here R/R_0 is plotted as a function of the volume fraction of crowders ϕ_c (left) and their number density ρ_c (right). Note that unless otherwise stated, lengths are measured in units of $\sigma = a$, as is the case for Fig. 2–6.

As shown in the graph on the left in Fig. 2(a), the polymer chain shrinks in size as the volume fraction of crowding agents ϕ_c increases as long as $a_c < 0.6a$. They induce entropic attractions, often referred to as depletion forces, between monomers that would otherwise repel each other, swelling the chain (see ref. 13–15 for the nature of these forces in a more general context as well as ref. 39 and 40 for chain compaction in an unconfined space or in a poor solvent). With smaller crowders, the chain is compacted at a smaller volume fraction. This also explains why too large ones fail to condense the chain (shown in grey); they are ineffective. On the other hand, on a density basis, larger ones condense the chain more effectively except for $a_c = 0.6a, 0.8a$. For too large a_c , the desired value of ρ_c for compaction cannot be reached.

These findings are in qualitative agreement with the physical picture illustrated on the right in Fig. 1. Each monomer is surrounded with a ‘depletion layer’, described by a dashed line, in which the center of crowders is not accessible.¹⁵ Overlapping of depletion layers allows the surrounding crowders to explore a larger space. The resulting entropic (depletion) force is related to V_{overlap} , the volume of the overlapped (shaded) region between two monomers. If r is the center-to-center distance of two adjacent monomers, $V_{\text{overlap}}(r) = \frac{\pi}{6}(a + a_c - r)^2(a + a_c + r/2)$ with its maximum given by $V_{\text{overlap}}(r = a) = \frac{\pi}{6}a_c^2(3a/2 + a_c) \equiv \Delta V_{\text{max}}$.¹⁵ Let Π_c be

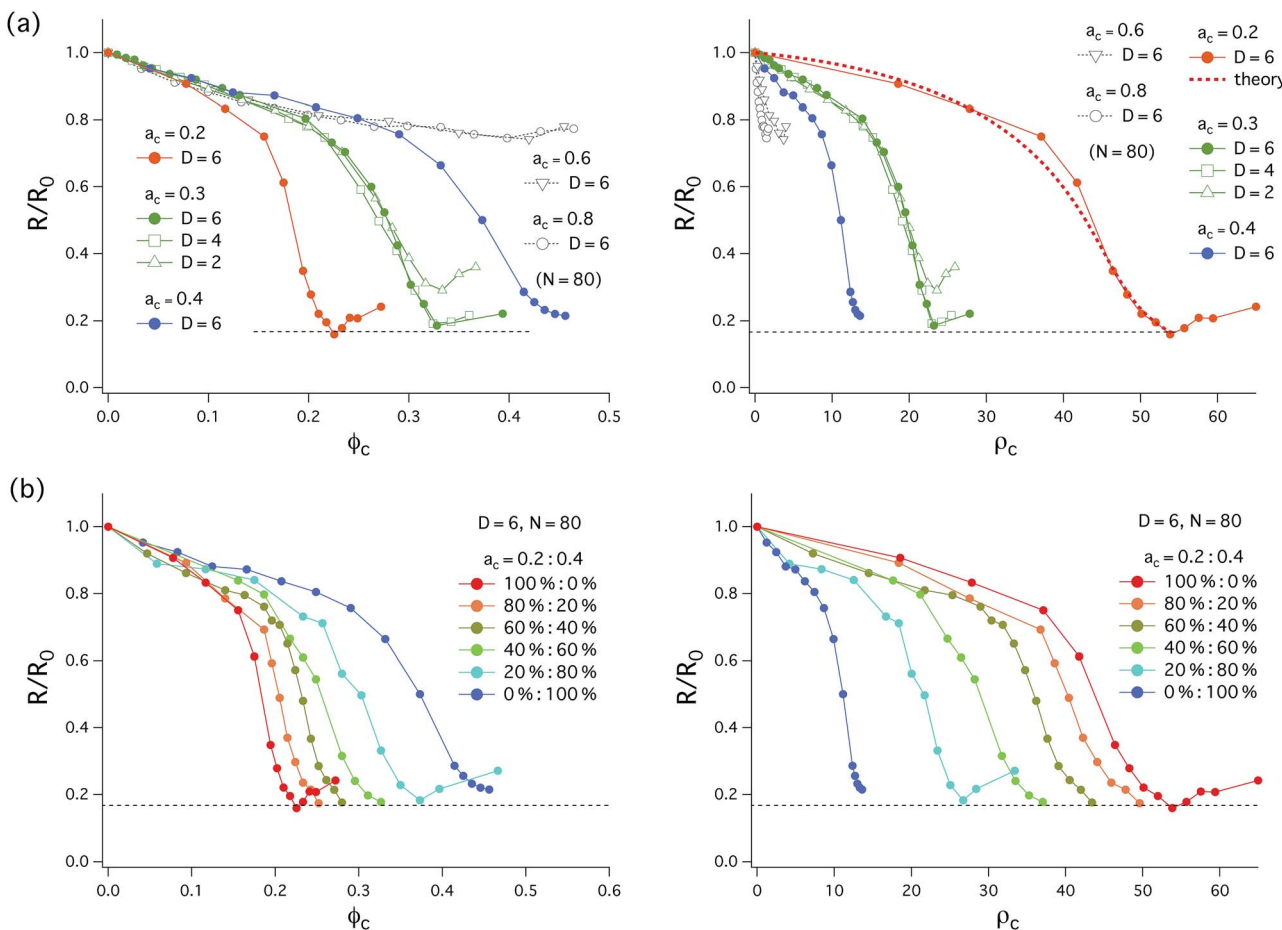


Fig. 2 Collapse of a flexible chain ($N = 80$) by crowding agents in a cylindrical space as a function of the volume fraction ϕ_c (left) and the density ρ_c (right) of crowding particles for the mono-disperse (a) and poly-disperse case (b). (a) As ϕ_c or ρ_c increases, the confined chain shrinks in size. Here, R/R_0 is the reduced chain size with R_0 being the equilibrium size in the absence of crowding particles. The chain size reaches a minimum at a certain value of ϕ_c or ρ_c . A few curves for $a_c = 0.3$ corresponding to different D values (green) tend to collapse onto each other. This implies that cylindrical confinement enters into the picture through R_0 . The dotted line was obtained using a free energy approach (see Subsection 3.4). (b) In the presence of a mixture of small ($a_c = 0.2$) and large ($a_c = 0.4$) crowders, chain compaction appears to interpolate the two corresponding mono-disperse cases, each containing one kind of crowder (see Fig. 4 for details). As a result, the polydispersity of crowders does not alter chain compaction qualitatively.

the osmotic pressure of crowders in a monomer-free region, then the depletion force between two monomers can be obtained approximately as $f_{\text{dep}} \approx \Pi_c \times \partial V_{\text{overlap}} / \partial r$. Of particular interest is the maximum free energy gain of two monomers, which is reached when they are brought in contact,

$$\Delta F_{\max} \approx \rho_c \Delta V_{\max} \sim \begin{cases} \rho_c a_c^2 (3a/2 + a_c) \\ \phi_c (1 + 3a/2a_c) \end{cases} \quad (3)$$

Note that this is an approximation, since ΔV_{\max} is obtained for two monomers while others are ignored; at best, ΔF_{\max} is correct at the level of two-body interactions and at a low density of crowders. As the density of crowders increases, higher-order terms (e.g., ρ_c^2) will have to be included (see eqn (8)). Also two adjacent monomers do not have to be in contact, as assumed for the quantity ΔV_{\max} .

Despite its limitation, the relation in eqn (3) appears to explain the general trend seen in our observation in Fig. 2: on the basis of ϕ_c , smaller particles are more effective crowders, while on a density basis, the opposite is true. A more complete analysis is presented below (see Fig. 4).

Chain swelling beyond the complete compaction (Fig. 2) is a simulation artifact. In our simulation, the initial conformation was chosen to be helically elongated. At sufficiently high ϕ_c , which is larger than needed for the full compaction, the chain got trapped in a local minimum. This makes the global chain equilibrium time longer than typical simulation times. A similar non-monotonic dependence was observed in chain compaction by crowders in bulk.²³ This is, however, distinct from the non-monotonic dependence of chain sizes on ϕ_c observed in an earlier study, in which crowders were implicitly included.⁴¹ As pointed out,⁴² this non-monotonicity can be attributed to the implicit presence of crowders through

theoretically-obtained depletion forces. In our study and in ref. 23 and 42 explicit crowders were used.

Chain compaction as shown in Fig. 2 and 4 appears to be a continuous transition. Because of finite-chain lengths, however, this is not so conclusive. To further clarify this, we have used a theoretical approach and presented it in Subsection 3.4. As described by the dashed curve in the graph on the right in Fig. 2(a), our theoretical results are in excellent agreement with the data, indicating a continuous transition, similarly to the theoretical analysis in ref. 16 (see Subsection 3.5 for more detailed discussions).

Fig. 3 shows our results for the probability distribution (left) and the variance (right) of chain sizes, denoted as $P(R)$ and σ_R^2 , respectively; on the right graph, chain compaction (left axis) is related to the variance σ_R^2 (right axis), as a function of ϕ_c . The width of $P(R)$ is essentially σ_R . The results in Fig. 3 supplement those in Fig. 2. First, in all cases, $P(R/R_0)$ has a single peak or is unimodal, similarly to what was observed in an unconfined space.²³ While this is consistent with the results in Fig. 2, in that it does not support a coexistence of extended and collapsed states, because of the finite value of $N = 80$, however, this is not so decisive.

The results in Fig. 3 also show how chain compaction suppresses its conformational fluctuation and “stiffens” the chain. Note that the effective spring constant of a polymer chain is reciprocally related to σ_R^2 as $k_{\text{eff}} \sim 1/\sigma_R^2$.^{33,35} When compacted, the chain becomes a stronger spring, as evidenced by reduced σ_R^2 values (blue squares) for large ϕ_c values; k_{eff} increases by up to about seventy fold or almost by two orders of magnitude.

So far, we have focused our discussion on a mono-disperse case, *i.e.*, all crowding particles having the same size. To mimic the cellular environment more realistically, we have also considered a mixture of small ($a_c = 0.2$) and large ($a_c = 0.4$)

crowding particles with their relative volume fractions ranging from (20% : 80%) to (80% : 20%). Fig. 2(b) shows our results for this poly-disperse case, which appears to interpolate the two respective mono-disperse cases; poly-dispersity does not change chain compaction qualitatively.

How are a_c and ρ_c intertwined? Fig. 4 shows the interplay between crowder size a_c and density ρ_c for the mono-disperse (left) and poly(bi)-disperse cases (right). The size of a flexible chain ($N = 80$) in a cylindrical space is displayed as a function of the rescaled variable $a_c^2 \rho_c$ for the mono-disperse (left) or $\sum a_c^2 \rho_c$ for the poly-disperse case (right), where the sum is to be carried out over two types of crowders:

$$\sum a_c^2 \rho_c = a_{\text{small}}^2 \rho_{\text{small}} + a_{\text{large}}^2 \rho_{\text{large}}. \quad (4)$$

(Here and below, for simplicity, a_c is given in units of a , especially when it refers to simulation results.) (Left) When plotted against $a_c^2 \rho_c$, the curves corresponding to different values of a_c collapse onto each other. As a result, doubling a_c is equivalent to increasing ρ_c fourfold.

For the poly-disperse case (on the right), we use a mixture of small ($a_c = 0.2$) and large ($a_c = 0.4$) crowders with a varying range of their volume fractions, $\{(80\% : 20\%), \dots, (20\% : 80\%)\}$, and $\{(97\% : 3\%), \dots, (67\% : 33\%)\}$ are the corresponding number fractions. Let x be the number fraction of small crowders, then eqn (4) can be rewritten as

$$\sum a_c^2 \rho_c = [x a_{\text{small}}^2 + (1 - x) a_{\text{large}}^2] \rho_c^{\text{total}}, \quad (5)$$

where $\rho_c^{\text{total}} = \rho_{\text{small}} + \rho_{\text{large}}$ and $x = \rho_{\text{small}}/\rho_c^{\text{total}}$. This relation leads to $(0.97 a_{\text{small}}^2 + 0.03 a_{\text{large}}^2) \rho_c^{\text{total}}$ for the volume-fraction mixture (80% : 20%). Our results on the right in Fig. 4 suggest that the effect of poly-dispersity can be correctly mimicked by adjusting the size of crowders in a homogeneous-crowder system, according to our rescaling scheme in eqn (4) or (5).

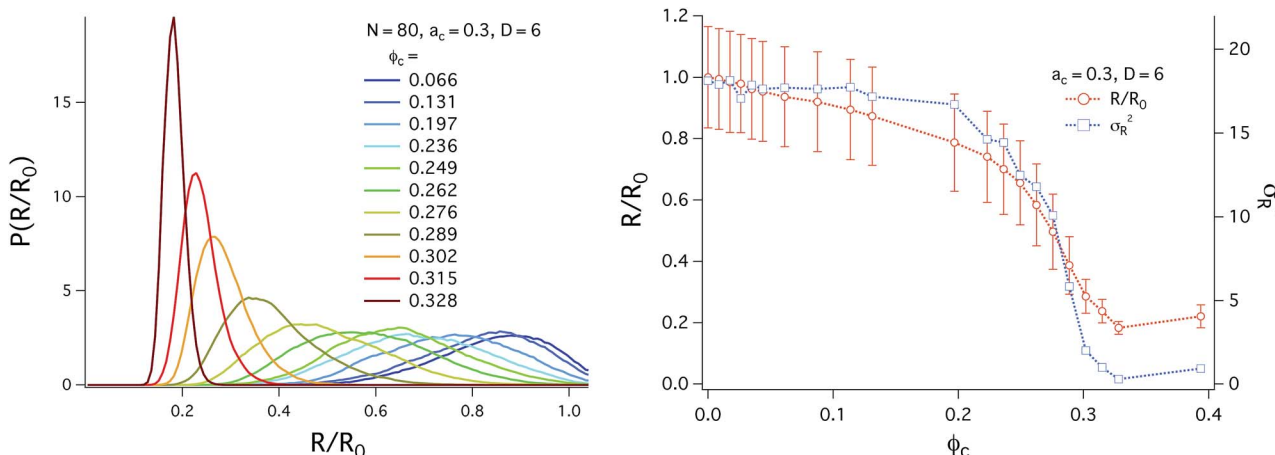


Fig. 3 Chain size distributions (left) and variances (right) of a confined chain in the presence of crowders. (Note here that lengths are given in units of a .) (left) The probability distribution of the reduced chain length R/R_0 , denoted as $P(R/R_0)$, is displayed as a function of R/R_0 for various choices of ϕ_c . In all these cases, $P(R/R_0)$ is unimodal, meaning that the system remains in a single phase, either extended (for small ϕ_c values) or condensed (for large ϕ_c values). As ϕ_c increases, the conformational fluctuation becomes frozen, as measured by the width of each curve. (right) Chain compaction (left axis) is contrasted with the variance σ_R^2 (right axis), as a function of ϕ_c ; the width of $P(R)$ determines σ_R^2 . The effective spring constant of the chain k_{eff} is related to σ_R^2 as $k_{\text{eff}} \sim 1/\sigma_R^2$. This graph suggests that chain compaction can “stiffen” the chain up to about seventy fold, as evidenced by much reduced σ_R^2 values (or much increased k_{eff} values) for large ϕ_c values.

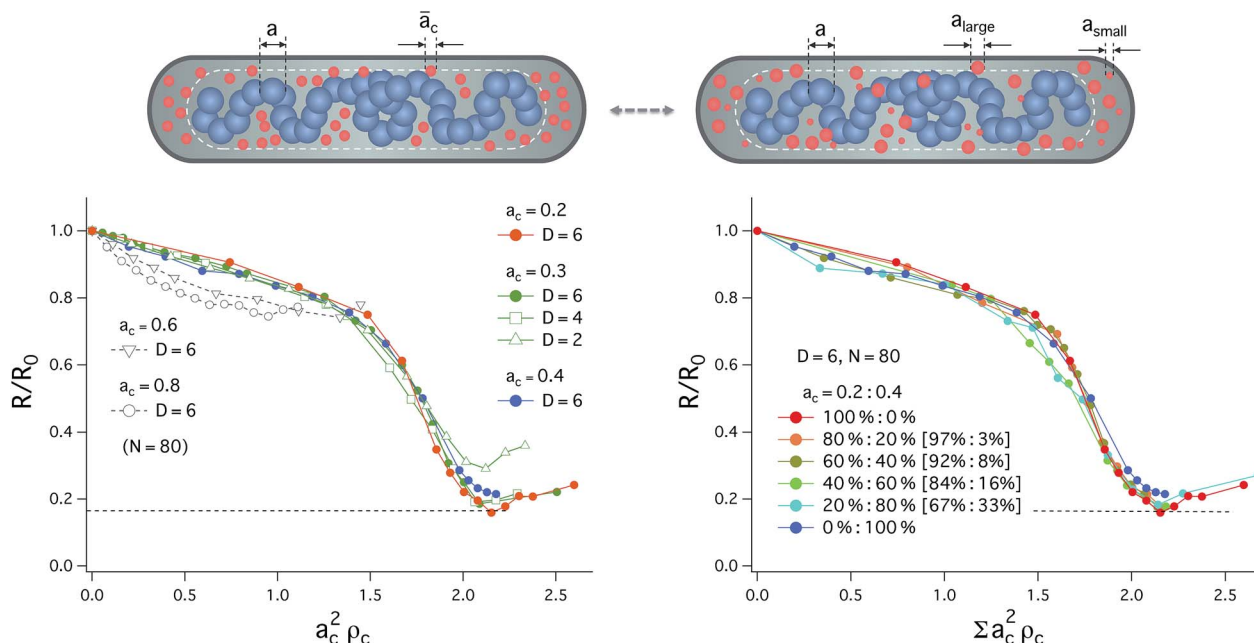


Fig. 4 The interplay between crowder size and density for the mono-disperse (left) and poly-disperse cases (right). (Note here that lengths are given in units of a .) The size of a flexible chain ($N = 80$) in a cylindrical space is displayed as a function of the rescaled variable $a_c^2 \rho_c$ for the mono-disperse (left) or $\sum a_c^2 \rho_c$ for the poly-disperse case (right). (Left) When plotted against $a_c^2 \rho_c$, the curves corresponding to different values of a_c collapse onto each other. As a result, doubling a_c is equivalent to increasing ρ_c fourfold. For the polydisperse case (on the right), we use a mixture of small ($a_c = 0.2$) and large ($a_c = 0.4$) crowders with a varying range of their volume fractions $\{(80\% : 20\%), \dots, (20\% : 80\%) ; \{97\% : 3\%, \dots, (67\% : 33\%\}$) are the corresponding number fractions, respectively. Here, $\sum a_c^2 \rho_c = a_{\text{small}}^2 \rho_{\text{small}} + a_{\text{large}}^2 \rho_{\text{large}}$, e.g., $0.97a_{\text{small}}^2 \rho_{\text{small}} + 0.03a_{\text{large}}^2 \rho_{\text{large}}$ for the volume-fraction mixture (80% : 20%). Our results on the right suggest that the effect of polydispersity can be mimicked by adjusting the size of crowders in a homogeneous-crowder system, according to our rescaling scheme $\sum a_c^2 \rho_c = a_{\text{small}}^2 \rho_{\text{small}} + a_{\text{large}}^2 \rho_{\text{large}}$.

While it is not entirely clear why a_c^2 or $[xa_{\text{small}}^2 + (1 - x)a_{\text{large}}^2]$ is the correct rescaling factor, eqn (3) offers some insight though not complete. When we used $a_c^2(3a/2 + a_c)$ from eqn (3) as a rescaling factor for the mono-disperse case, the collapse between different compaction curves was somewhat worse than in the results in Fig. 4 (data not shown). Considering the limitations of eqn (3) as discussed earlier, this is understandable.

Our findings in Fig. 4 will be useful for interpreting experimental data and for making predictions, especially for a polydisperse case. In particular, they enable us to define an “average” crowder size \bar{a}_c and the density of average crowders $\bar{\rho}_c$, as illustrated on the top panel in Fig. 4:

$$\bar{a}_c^2 \bar{\rho}_c = \sum a_c^2 \rho_c = a_{\text{small}}^2 \rho_{\text{small}} + a_{\text{large}}^2 \rho_{\text{large}}. \quad (6)$$

Note here that what this relation determines is the combination $\bar{a}_c^2 \bar{\rho}_c$. This means that the corresponding mono-disperse case is not uniquely determined. One possibility is to use the same number of crowders in the mono-disperse case: $\bar{\rho}_c = \rho_{\text{small}} + \rho_{\text{large}}$. Then eqn (6) becomes

$$\bar{a}_c^2 = xa_{\text{small}}^2 + (1 - x)a_{\text{large}}^2. \quad (7)$$

(Recall that x is the number fraction of small crowders.) Extended analysis along this line will be useful for making quantitative sense of cytoplasmic crowders, which present a poly-disperse system.^{4,5}

3.2 Phase separations

We have also considered how the system phase-separates into crowder-rich and chain-rich phases. Unlike a corresponding system in an unconfined space, the phase separation in this case will be anisotropic. Accordingly, we have calculated the spatial distribution of monomers and crowding particles along the long symmetry axis of the cylinder as well as in the radial direction, denoted as ρ_z and ρ_r , respectively; for ρ_z , the center of mass of a chain is assumed to be located at $z = 0$.

Fig. 5 shows our results for ρ_z (left) and ρ_r (right) for the polydisperse case $a_c = 0.2 : 0.4$ (40% : 60%), corresponding to the green line in Fig. 2(b) ($N = 80$ and $D = 6$). The rescaling factor ρ_{ref} used for the left graph is chosen to be $\rho_z(z = \infty)$ for crowders and $\rho_z(z = 0)$ for the chain. (Here ρ_{ref} for $a_c = 0.2$ is defined independently of that for $a_c = 0.4$.) The introduction of ρ_{ref} is merely to enhance the visibility of the graph. On the other hand, ρ_r on the right is a normalized one: $\int \rho_r 2\pi r dr = 1$, which is satisfied separately by small and large crowders, and monomers. For sufficiently large ϕ_c values (all curves displayed except for $\phi_c = 0.155$), crowders are effectively depleted from the chain-rich phase. But the boundary between the two phases is smooth, somewhat distinct from a sharp one assumed in a theoretical approach (see the SI of ref. 16 and references therein).

The graph on the right in Fig. 5 shows how crowders and monomers are spatially distributed along the radial direction. In contrast to ρ_z , the radial distribution ρ_r , especially for monomers, does not appear to be sensitive to the degree of

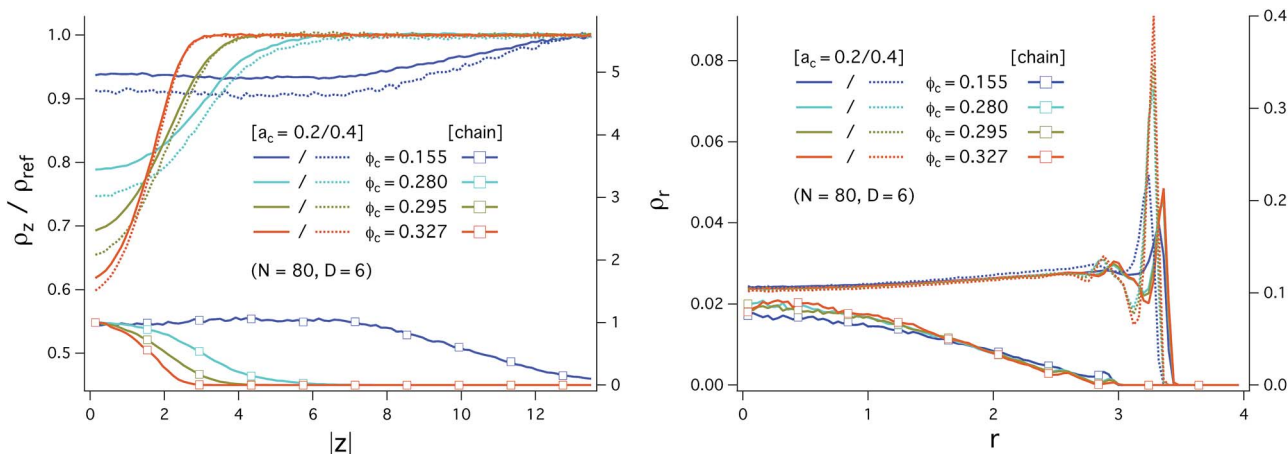


Fig. 5 Phase separation into crowder-rich and chain-rich phases in the longitudinal (left) and transverse direction (right) for $N = 80$ and $D = 6$. (Note here that lengths are given in units of a .) For this, we have calculated the spatial distribution of crowding particles and monomers along the long symmetry axis of the cylinder and in the radial direction, denoted as ρ_z and ρ_r , respectively, for the poly-disperse case $a_c = 0.2 : 0.4$ (40% : 60%), corresponding to the green line in Fig. 2(b); for ρ_z , the center of mass of a chain is assumed to be located at $z = 0$. The rescaling factor ρ_{ref} used for the left graph is defined as $\rho_z(z = \infty)$ for crowders and $\rho_z(z = 0)$ for the chain; the ρ_{ref} values for small and large crowders are constructed independently. This is merely to enhance the visibility of the graph. On the other hand, ρ_r on the right is normalized: $\int \rho_r 2\pi r dr = 1$ (this is satisfied separately by small and large crowders, and monomers). For sufficiently large ϕ_c , crowders are effectively depleted from the chain-rich phase, even though ρ_z changes continuously as a function of z . In contrast to ρ_z , ρ_r is not so sensitive to ϕ_c , especially for monomers; wall-layering of crowders is more pronounced for larger ϕ_c values. Our results here suggest that chain compaction occurs mostly in the longitudinal direction.

chain compaction. The main effect is to enhance the depletion of monomers from the cylindrical wall (see ref. 22 for a similar observation with DNA). However, this effect appears to be minor in our flexible-chain case, compared to what was seen with DNA molecules. This means that flexible-chain compaction occurs mainly along the long axis of the cylinder. This justifies the (quasi) one-dimensional approach to chain compaction in a cylindrical space in ref. 16 and in Subsection 3.4.

Because of the wall-monomer repulsion, ρ_r for the chain is maximized at $r = 0$, similarly to the corresponding case without crowders.^{33,35} The opposite is expected for the crowders. Even for $\phi_c = 0.155$, which is not sufficient to compact the chain, cylinder-wall layering of crowders is apparent, similarly to the layering of monomers in the absence of crowders.³⁵ Also varying the size of crowders does not alter ρ_z and ρ_r qualitatively.

3.3 Chain compaction vs. adsorption

So far, we have used $\varepsilon_{13} = 5.0$, the strength for the interaction between monomers and the cylinder wall, so as to mimic the experimental setting in ref. 16, where the cylinder wall was passivated with PLL-g-PEG [poly(L-lysine)-g-poly(ethylene glycol)]. As a result, chain adsorption was discouraged. This appears to be consistent with the picture of bacterial chromosomes as self-adherent or coherently-shaped objects rather than cell-membrane sticking ones.^{43,44} However, it is not clear if this is a deceptive parallel, since the local organization of chromosomes involves various nucleoid-associated proteins. To further clarify the role of depletion forces in organizing confined polymers, it will be useful to examine chain compaction with varying ε_{13} .

Under different conditions, crowders can induce depletion forces between a monomer and the cylindrical wall, possibly leading to chain adsorption. To understand the interplay between chain compaction and adsorption, we have examined the consequence of varying ε_{13} and plotted our results in Fig. 6. We have chosen the parameter so that the chain is collapsed for large ε_{13} values, including $\varepsilon_{13} = 5.0$ used for the previous results in Fig. 2 and 4 as well as in Fig. 5, assuming that the volume fraction of crowders is sufficiently large. The results in Fig. 6(a) and (b) remain roughly insensitive to ε_{13} , as long as $\varepsilon_{13} \geq 2.0$ (a) or $\varepsilon_{13} \geq 3.0$ (b). For $\varepsilon_{13} = 1.0$, the chain is elongated along the long axis of the cylinder as shown in Fig. 6(a), similarly to what is observed for sufficiently small ϕ_c and $\varepsilon_{13} = 5.0$. In contrast to the latter case, the resulting ρ_r in Fig. 6(b) is single-peaked at $r \approx D/2$ ($\int \rho_r 2\pi r dr = 1$). This is reminiscent of strong chain adsorption onto the cylinder wall; most of the monomers are trapped in a thin layer of thickness comparable to a_c at $r \approx D/2$ (see Fig. 6(b)). The crowding particles induce depletion attractions between monomers and the wall, which turn out to be stronger than the attraction between monomers.

For $\varepsilon_{13} = 2.0$, the chain is both compacted and adsorbed onto the wall; the tendencies for adsorption and compaction are comparable. This is responsible for the oscillatory behavior of ρ_r for $\varepsilon_{13} = 2.0$ in Fig. 6(b). Imagine increasing ε_{13} from $\varepsilon_{13} = 1.0$ (complete adsorption), thus reducing the adsorption tendency. Some of the monomers become more loosely bound and leave the adsorption layer, forming a layer right next to the adsorption layer. Depending on the balance between adsorption and compaction, multiple layers can form, giving rise to an oscillatory behavior of ρ_r as shown in Fig. 6(b).

Chain adsorption can alter chain conformation and thus R . The graph in Fig. 6(c) shows how chain adsorption and chain

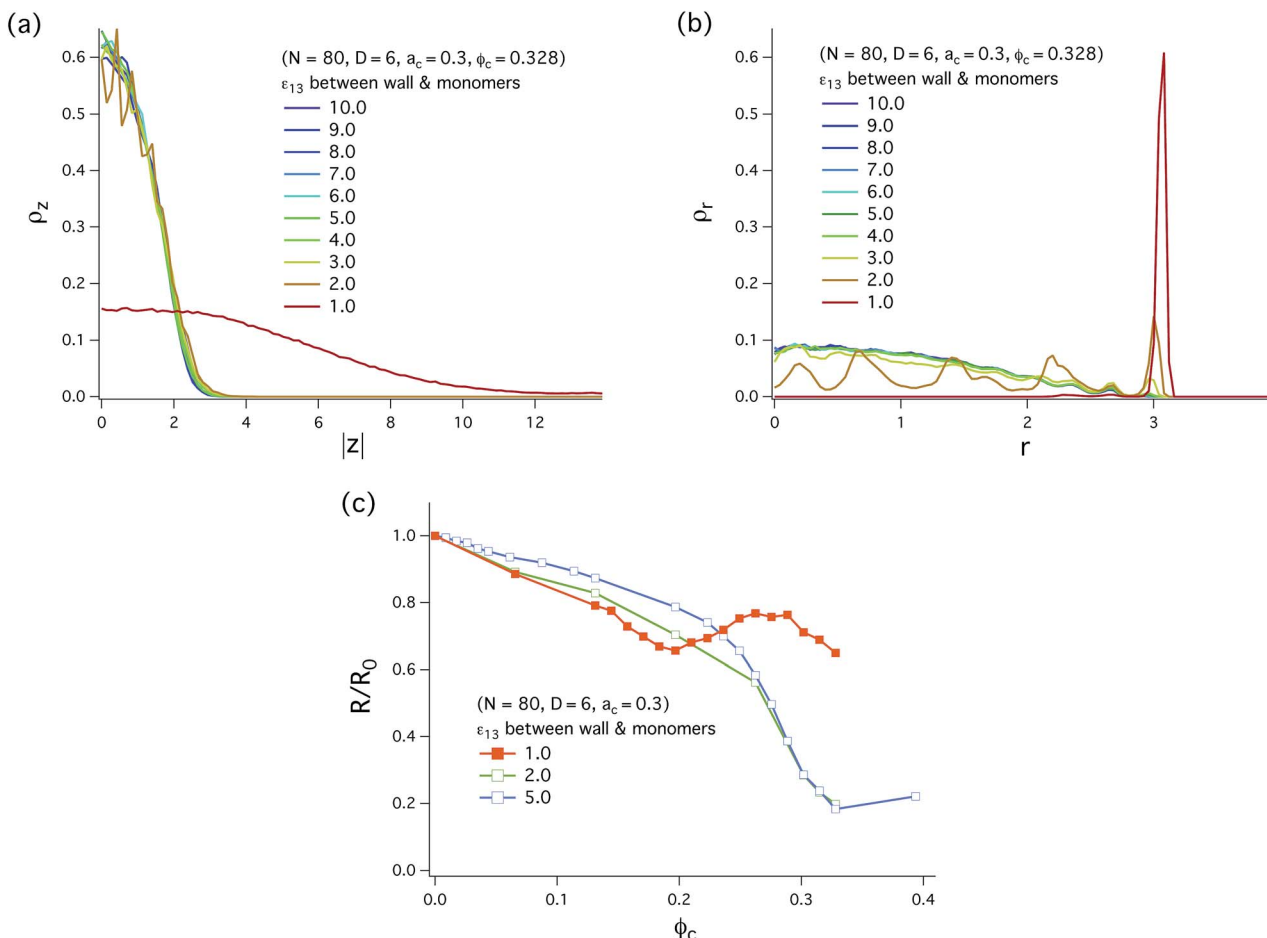


Fig. 6 The interplay between chain compaction and adsorption: how to choose ϵ_{13} , i.e., the interaction strength between monomers and the cylinder wall. (Note here that lengths are given in units of a .) The graphs in (a) and (b) display ρ_z or ρ_r , respectively, for a wide range of ϵ_{13} ; ρ_r is normalized so that $\int \rho_r 2\pi r dr = 1$. Other parameters have been chosen so that the chain is collapsed for large ϵ_{13} values, including $\epsilon_{13} = 5.0$ used for the previous results in Fig. 2 and 4 as well as in Fig. 5. The results remain roughly insensitive to ϵ_{13} as long as $\epsilon_{13} \geq 2.0$ (left) or $\epsilon_{13} \geq 3.0$ (right). For $\epsilon_{13} = 1.0$, the chain is elongated along the long axis of the cylinder, similarly to what is observed for sufficiently small ϕ_c and $\epsilon_{13} = 5.0$; on the other hand, the resulting ρ_r is single-peaked at $r \approx D/2$. This finding can be attributed to chain adsorption onto the cylinder wall. The crowding particles induce stronger attractions between monomers and the wall. For $\epsilon_{13} = 2.0$, on the other hand, the chain is both compacted and adsorbed onto the wall. For larger ϵ_{13} , however, adsorption is discouraged. The graph in (c) summarizes the effect of adsorption on chain compaction. For $\epsilon_{13} = 1.0$, a reentrant-like transition occurs: the confined chain initially shrinks in size as ϕ_c increases from 0, stretches with increasing ϕ_c in its intermediate range, and eventually becomes more compact, but not as effectively as in other cases ($\epsilon_{13} = 2.0, 5.0$). This observation is correlated with our results in (a) and (b). For $\epsilon_{13} = 2, 3, \dots$, adsorption will not complicate chain compaction (see (a)), but for $\epsilon_{13} = 1.0$, the competition between compaction and adsorption leads to a reentrant-like transition. In the intermediate- ϕ_c range, i.e., $0.2 < \phi_c < 0.3$, chain adsorption (see (b)) promotes chain stretching.

compaction are intertwined. For $\epsilon_{13} = 1.0$, a reentrant-like transition occurs. Molecular crowding condenses the confined chain initially for small ϕ_c but rather stretches it in some intermediate range of ϕ_c . (See ref. 45 and 46 for a similar but somewhat distinct reentrant coil-globule-coil transition of a polymer chain.) For large ϕ_c , the chain becomes more compact with increasing ϕ_c but not as effectively as in other cases ($\epsilon_{13} = 2.0, 5.0$). This observation can be understood in light of our results in Fig. 6(a) and (b). For $\epsilon_{13} = 2, 3, \dots$, the interdependence between adsorption and compaction is insignificant (see Fig. 6(a)). For $\epsilon_{13} = 1.0$, however, crowders can induce chain adsorption (see Fig. 6(b)), promoting chain stretching in the intermediate- ϕ_c range, i.e., $0.2 < \phi_c < 0.3$.

3.4 Free energy approach

As a fitting model, here we present a free-energy approach, in which the chain size R can be obtained by free-energy minimization. Using this, we fit our simulation data for R . Let V be the “enveloping” volume of the chain, inside which the chain is enclosed possibly together with crowding agents (see the dashed line in Fig. 1). As the chain is compacted, V decreases. Let m be the number of crowders within V . If we ignore boundary effects, the total free energy of the subsystem enclosed within V (or the chain-rich phase) is given by

$$\frac{F_{\text{total}}}{k_B T} = \underline{m \ln \frac{m}{V}} - m + B_2 \frac{m^2}{V} + \frac{5}{8} B_2^2 \frac{m^3}{2V^2} + \frac{A}{D} \left(\frac{R_0^2}{R} + \frac{R^2}{2R_0} \right) + \frac{N^3 a^6}{R^2 D^4} + F_{\text{dep}}. \quad (8)$$

Various terms and symbols are defined as follows. The underlined term describes the corresponding crowder-only system (F_{crowd}) (see for instance ref. 47), where B_2 is the second virial coefficient given by

$$B_2 = 4 \times \frac{4\pi}{3} \left(\frac{a_c}{2} \right)^3. \quad (9)$$

The relevance of higher-order terms can be checked *a posteriori*.[‡]

The next term is the (renormalized) Flory free energy of a confined chain in the absence of crowders;⁴⁸ in this expression, A is a numerical prefactor, which can be adjusted for the best fit to numerical data. The second-last term is a standard three-body interaction energy, which is needed when the chain is significantly compressed. Unlike the two-body term included in the term containing A , which describes blob–blob overlap free energy, this term captures monomer–monomer interactions. This term is needed to avoid a complete collapse of the chain or $R \approx 0$; the notion of blobs becomes less meaningful.[§]

Furthermore, F_{dep} is the free energy reduction due to the depletion of crowding agents from the chain and is related to F_{crowd} :

$$F_{\text{dep}} = V_{\text{dep}} \left(- \frac{\partial F_{\text{crowd}}}{\partial V} \right) = V_{\text{dep}} \Pi_c. \quad (10)$$

Here V_{dep} is the volume of the depletion zone and Π_c is the osmotic pressure of crowders. A standard choice of V_{dep} per monomer for beads on a string is given by

$$\begin{aligned} V_{\text{dep}} &= \frac{4\pi}{3} \left(\frac{a + a_c}{2} \right)^3 - \Delta V_{\max} \\ &= \frac{\pi}{12} a (2a^2 + 6aa_c + 3a_c^2). \end{aligned} \quad (11)$$

Note that the volume of each monomer is included as in ref. 9–11.

On the other hand, the free energy of the system outside the volume V is mainly determined by crowders and is similar to the

[‡] The term containing m^3 here is in part to improve the agreement between our theoretical and numerical results. Without this term, a larger value of A has to be used. See the relevant discussion after eqn (12). Also this is analogous to the three-body term for a polymer chain, *i.e.*, the second-last term in eqn (8).

[§] It is worth mentioning that the choice of this term does not influence the nature of compaction by crowders. This is in sharp contrast to chain collapse in a poor solvent, for which the coefficient of this term dictates the nature of chain collapse (continuous *vs.* abrupt).⁴⁹ If we constructed this term based on blob–blob interactions, the D dependence would be different. Together with insensitivity of chain compaction to the numerical prefactor of this term, this suggests that the details of this term are not reflected sensitively in chain compaction in a crowded medium. Also note that this discussion is limited to a flexible chain and does not necessarily contradict the observation of an abrupt collapse of DNA in a tube.^{21,22}

underlined term in eqn (8) denoted as F_{crowd} , except that V should be replaced by the total volume of the cylinder minus V and m by the total number of crowders minus m .

In equilibrium, there will be chemical and mechanical equilibrium across the boundary of the volume V . Let μ_i and Π_i be the chemical potential and osmotic pressure of crowders, respectively, where $i = \text{'in' or 'out'}$. In equilibrium,

$$\mu_{\text{in}} = \mu_{\text{out}} \text{ and } \Pi_{\text{in}} = \Pi_{\text{out}}. \quad (12)$$

For our analysis, we assumed that $V = R \times \pi(D/2)^2$ and minimized F_{total} with respect to R and m_i ($i = \text{in or out}$). Also we tried two choices of V_{dep} per monomer: the one given in eqn (11) and $V_{\text{dep}} = \frac{4\pi}{3} \left(\frac{a}{2} \right)^3$, *i.e.*, the volume around the chain inside which crowders are depleted. For some reason, the latter choice leads to a better quantitative agreement with our simulation data. The red dashed line in the graph on the right in Fig. 2(a) was obtained with this choice and $A = 2.84 \times 6$. Note that this value is about six times the one reported in ref. 48. On the other hand, when V_{dep} in eqn (11) was used instead, we had to use a much larger A value for the best fit to the data. In our theoretical approach, we used step-wise distributions of crowders and monomers in contrast to what our results in Fig. 5 suggest. Some quantitative disagreement is thus expected. This numerical prefactor changes the transition only quantitatively. We thus content ourselves with a qualitative agreement between theory and simulations.

3.5 Chain compaction: continuous or abrupt

Our theoretical analysis, which is relevant for the long-chain limit, suggests that the compaction transition by crowding agents in a cylindrical space is continuous. This finding is consistent with our simulation results in Fig. 2 (as well as in Fig. 3 (left)). It appears that finite-chain size effects would not alter the transition qualitatively. However, it is distinct from the observation that “naked” DNA molecules undergo an abrupt compaction under cylindrical confinement but a continuous compaction in a slit-like and free space.^{21,22} This suggests that the geometry of confined spaces is well reflected in the way crowders collapse chain molecules.

Intriguingly, DNA molecules under slit-like and tube confinement were seen to elongate initially with increasing concentration of crowders, before they eventually collapsed.^{21,22} To account for this, one can rely on the physical picture that DNA segments are depleted in a (depletion) layer of some thickness on the order of ℓ_p from the confining wall, where $\ell_p \approx 500 \text{ \AA}$ is the persistence length of DNA.^{21,22} This allows for an easy access of crowders in this depletion layer, effectively increasing the degree of confinement – more so for a larger ℓ_p .

This explains the initial elongation of DNA molecules under confinement, more effectively for the tube geometry; this non-monotonic behavior was viewed as underlying the abrupt transition in the tube confinement.^{21,22} It also implies that chain flexibility can delay or even prevent the emergence of this effect, as seen in Fig. 2.

In contrast to the DNA case, the compaction of *E. coli* chromosomes in the tube confinement appears to be monotonic.¹⁶ In other words, chain-segment depletion from the confining wall, which was seen in the former case, does not appear to be correlated with the observation of coexisting phases in the chromosome experiment, *i.e.*, chromosome-rich and crowder-rich phases,¹⁶ which would be nominally interpreted as a signature of abrupt (first-order) phase transitions. Thus, it is not entirely clear whether the phase coexistence arises from chain stiffness or chain heterogeneity.¶ Imagine a chain molecule consisting of two regions parameterized by different values of A (see eqn (8)). At some value of ϕ_c , it is possible that one region which is almost fully-compacted can coexist with the other in an extended conformation. This, however, does not necessarily mean that the transition is either continuous or abrupt. For further clarifying the nature of compaction, one should include other biological details that our model leaves out.

Along this line, it is worth mentioning that the bacterial chromosome resembles a confined chain, as demonstrated in ref. 16; monomers in our study should be interpreted as a coarse-grained model of the structural units of the bacterial chromosome, each consisting of supercoiled DNA strands and DNA-associated proteins^{1,16,19,20} (see the illustration in Fig. 1). Beyond this general picture, the details, best characterized for the *E. coli* nucleoid, vary from reference to reference (see ref. 16, 19 and 20). For instance, early measurements suggest that the size of each unit is $a_{\text{unit}} = 70 \pm 20 \text{ nm}$ and the number of units falls around $n_{\text{unit}} = 100$.¹⁹ In a more recent estimate, $a_{\text{unit}} = 100\text{--}400 \text{ nm}$ and $n_{\text{unit}} = 63\text{--}284$ per cell (15–65 per chromosome).¹⁶ Our choice of $N = 80$ falls in the acceptable range. Also recall that in our simulations we used a (monomer size) as length units for other quantities such as a_c and D (see Section 4 for relevant discussions on our choice of a_c); on the other hand, we varied D so as to map out a general picture of how the degree of confinement is reflected in chain compaction, as shown in Fig. 2 and 4 (this effect becomes implicit if R is rescaled with R_0). Thus a thin semiflexible chain with a long persistence length may not necessarily describe the bacterial chromosome more adequately.

Indeed, a similar theoretical approach based on a flexible-chain model explains some feature of chromosome-compaction experiments, in which *E. coli* chromosomes were condensed by PEG (polyethylene glycol), which is a polymeric crowder like dextran.¹⁶ For instance, it produces a volume fraction of crowders required for compaction which is comparable to the experimental counterpart.

¶ Chain stiffness is not well known for the chromosome, since chromosome-bound proteins can modify the physical property of the DNA. As a result, our bead-spring model in Fig. 1 represents the chromosome better than it may seem at first glance.

4 Discussions and conclusions

In conclusion, we have examined how a flexible chain with self-avoidance is condensed by crowding particles in a (bacterial-cell-like) cylindrical space. Crowding particles induce entropic (depletion) forces between monomers, which compete with the direct repulsion between monomers. At a sufficiently high volume fraction of crowders, the depletion force is strong enough to collapse the chain, similarly to what was observed for bacterial chromosomes.¹⁶ The compaction appears to be rapid but continuous both in our simulation and in free energy analysis. To account for the phase coexistence seen in the recent experiment,¹⁶ a more realistic model chromosome will be desired, as noted above.

A salient feature of our results is the interplay between the size a_c and density ρ_c of crowders as summarized by the simple relation $a_c^2 \rho_c$ or $\sum a_c^2 \rho_c = a_{\text{small}}^2 \rho_{\text{small}} + a_{\text{large}}^2 \rho_{\text{large}}$ for a monodisperse or polydisperse case, respectively, against which chain compaction becomes independent of a_c or poly(bi)-dispersity (a_c given in units of a). According to this, in the monodisperse case, doubling a_c is equivalent to quadrupling ρ_c . Furthermore, the effect of polydispersity can be adequately mimicked by adjusting a_c in the corresponding monodisperse case. This finding, experimentally testable, can inspire new experiments. For instance, it will be useful to repeat the recent *E. coli* compaction experiment,¹⁶ using a poly-disperse mixture of crowders.

Because of the coarse-grained nature of our model nucleoid, one has to use due caution to test our results against experiments with the biological object: the nucleoid. For instance, our results suggest that the required volume fraction of crowders for full compaction is $\phi_c \approx 0.2$ (or 20%) when $a_c = 0.2$ (in units of a) is chosen. At first glance, this value appears to be in reasonable agreement with the volume fraction of “free” proteins in the cytoplasmic space ($\approx 12\text{--}17\%$) and that of PEG in *in vitro* experiments ($\approx 11\text{--}13\%$).^{2,16} However, the size of crowders also matters (see Fig. 2 and 4).

Considering that the size of structural units is in the range of $a \approx 100 \text{ nm}$ (up to 400 nm)¹⁶ and the size of proteins in the range of $a_c \approx 4.6 \text{ nm}$,^{1,12}|| $a_c = 0.046$ in units of a . On the other hand, $a_c^2 \rho_c \approx \phi_c/a_c$. Thus ($\phi_c = 10\%$, $a_c = 0.046$) maps onto ($\phi_c = 43\%$, $a_c = 0.2$). Taken literally, the cytoplasmic space has at least twice as many proteins as required for chromosome compaction (in addition to other biomolecules); the resulting depletion force can be strong enough to condense the chromosome.

In principle, one can improve the analysis above by correctly weighing various types of crowders in the computation of an average crowder size \bar{a}_c , assuming that eqn (6) or (7) works for a mixture of more than two kinds of crowders: $\bar{a}_c^2 \bar{\rho}_c = \sum a_c^2 \rho_c$, where the sum is over all types of crowders. Note here that what this relation determines is the combination $\bar{a}_c^2 \bar{\rho}_c$. Use of this rescaling relation for the cytoplasmic proteins would require

|| This is a typical size of cytoplasmic globular proteins. This is essentially identical to the known average protein size, 4 nm (or a radius of 2 nm).⁶

more complete knowledge about crowder sizes/densities in the cytoplasmic space.

Depending on parameter choices, crowders can induce attractions between monomers and the cylindrical wall, which are strong enough to induce chain adsorption, modifying the spatial distribution of monomers, especially in the radial direction. How this is implicated in chromosome organization is not obvious yet but can be explored.

Nevertheless, a physical picture emerging from our considerations is that depletion forces are as tangible as some other forces involved in biomolecular processes: hydrophobic forces responsible for the folding of proteins into their native structure⁴⁹ and counterion-induced attractions between DNA strands needed for DNA packing as in viruses.⁵⁰ Importantly, they are the main player in packing the bacterial chromosome. Indeed, the nature of these forces is as intriguing as that of electrostatic attractions between like-charged molecules.⁵⁰ To our mind, they are best caricatured as ‘attraction through repulsion’¹⁵ (see also Fig. 4 in ref. 16). New experiments under controlled conditions (e.g., crowder sizes and poly-dispersity) will be useful for further clarifying the nature of these forces and for testing our results.

As more computational power becomes available, one can use a more realistic model of chromosomes such as a semi-flexible-chain with crosslinks, interacting with crowders. Importantly, the favorable role of crowders goes beyond single-chromosome packing. It has been recently shown that they play an important role in properly partitioning two daughter chromosomes in a dividing bacterial cell.^{51,52} Our results reported here, especially for the poly-disperse case, will be useful for further appreciating the role of cytoplasmic crowders (with variable sizes) in organizing and segregating bacterial chromosomes.

Acknowledgements

We acknowledge financial support from the National Research Foundation of Korea (NRF: no. 2011-0028908 (H.J.) and no. 2012R1A1A2007488 (Y.J.)), the collaborative research contract funded by Korea Institute of Science and Technology Information (KISTI), and NSERC (Canada) (B.-Y.H.). This work was supported in part by the National Science Foundation Grant no. PHYS-1066293 and the hospitality of the Aspen Center for Physics. H.J. is grateful to the Supercomputing Center/KISTI for supercomputing resources. B.-Y.H. benefited from inspiring discussions with S. Jun and A. Grosberg.

References

- 1 See C. L. Woldringh and T. Odijk, in *Organization of the Prokaryotic Genome*, ed. R. L. Charlebois, ASM Press, Washington, D.C., 1999, and references therein.
- 2 J. A. Valkenburg and C. L. Woldringh, *J. Bacteriol.*, 1984, **160**, 1151–1157.
- 3 D. S. Goodsell, *Biochem. Mol. Biol. Educ.*, 2009, **37**, 325–332.
- 4 R. J. Ellis, *Trends Biochem. Sci.*, 2001, **26**, 597–604.
- 5 S. B. Zimmerman and A. P. Minton, *Annu. Rev. Biophys. Biomol. Struct.*, 1993, **22**, 27–65.
- 6 R. Phillips, *et al.*, *Physical Biology of the Cell*, Garland Science, 2nd edn, 2012.
- 7 H. Walter and D. E. Brooks, *FEBS Lett.*, 1995, **361**, 135–139.
- 8 J. Stavans and A. Oppenheim, *Phys. Biol.*, 2006, **3**, R1–R10.
- 9 R. de Vries, *Biophys. J.*, 2001, **80**, 1186–1194.
- 10 R. de Vries, *Biochimie*, 2010, **92**, 1715–1721.
- 11 S. Cunha, C. L. Woldringh and T. Odijk, *J. Struct. Biol.*, 2001, **136**, 53–66.
- 12 T. Odijk, *Biophys. Chem.*, 1998, **73**, 23–29.
- 13 S. Asakura and F. Oosawa, *J. Chem. Phys.*, 1954, **22**, 1255–1256.
- 14 S. Asakura and F. Oosawa, *J. Polym. Sci.*, 1958, **33**, 183–192.
- 15 H. N. W. Lekkerkerker and R. Tuinier, *Colloids and the Depletion Interaction*, Lecture Notes in Physics, Springer, 2011, vol. 833.
- 16 J. Pelletier, K. Halvorsen, B. Y. Ha, R. Paparcone, S. J. Sandler, C. L. Woldringh, W. P. Wong and S. Jun, *Proc. Natl. Acad. Sci. U. S. A.*, 2012, **109**, E2649–E2656.
- 17 X. Wang, P. M. Llopis and D. Z. Rudner, *Nat. Rev. Genet.*, 2013, **14**, 191–203.
- 18 V. G. Benza, B. Bassetti, K. D. Dorfman, V. F. Scolari, K. Bromeck, P. Cicuta and M. C. Lagomarsino, *Rep. Prog. Phys.*, 2012, **75**, 076602.
- 19 T. Romantsov, I. Fishov and O. Krichevsky, *Biophys. J.*, 2007, **92**, 2875–2884.
- 20 L. Postow, C. D. Hardy, J. Arsuaga and N. R. Cozzarelli, *Genes Dev.*, 2004, **18**, 1766–1779.
- 21 C. Zhang, P. G. Shao, J. A. van Kan and J. R. C. van der Maarel, *Proc. Natl. Acad. Sci. U. S. A.*, 2009, **106**, 16651–16656.
- 22 J. J. Jones, J. R. C. van der Maarel and P. S. Doyle, *Nano Lett.*, 2011, **11**, 5047–5053.
- 23 T. N. Shendruk, M. Bertrand, H. W. de Haan, J. L. Harden and G. W. Slater, 2014, arXiv:1407.2850v1 [cond-mat.soft].
- 24 D. Marenduzzo, C. Micheletti and P. R. Cook, *Biophys. J.*, 2006, **90**, 3712–3721.
- 25 S. Klump, M. Scott, S. Pedersen and T. Hwa, *Proc. Natl. Acad. Sci. U. S. A.*, 2013, **110**, 16754–16759.
- 26 B. R. Parry, I. V. Surovtsev, M. T. Cabeen, C. S. O’Hern, E. R. Dufresne and C. Jacobs-Wagner, *Cell*, 2014, **156**, 183–194.
- 27 J. D. Weeks, D. Chandler and H. C. Andersen, *J. Chem. Phys.*, 1971, **54**, 5237–5247.
- 28 K. Kremer and G. S. Grest, *J. Chem. Phys.*, 1990, **92**, 5057–5086.
- 29 G. S. Grest and K. Kremer, *Phys. Rev. A*, 1986, **33**, 3628–3631.
- 30 S. Jun and B. Mulder, *Proc. Natl. Acad. Sci. U. S. A.*, 2006, **103**, 12388–12393.
- 31 C. L. Woldringh, *Mol. Microbiol.*, 2002, **45**, 17–29.
- 32 Y. Jung, S. Jun and B. Y. Ha, *Phys. Rev. E: Stat., Nonlinear, Soft Matter Phys.*, 2009, **79**, 061912.
- 33 Y. Jung, C. Jeon, J. Kim, H. Jeong, S. Jun and B. Y. Ha, *Soft Matter*, 2012, **8**, 2095–2102.
- 34 S. Plimpton, *J. Comput. Phys.*, 1995, **117**, 1–19.
- 35 J. Kim, C. Jeon, H. Jeong, Y. Jung and B.-Y. Ha, *Soft Matter*, 2013, **9**, 6142–6150.
- 36 Y. Jung, C. Jeon, M. Ha and B.-Y. Ha, *Europhys. Lett.*, 2013, **104**, 68003.

- 37 P.-G. de Gennes, *Scaling Concepts in Polymer Physics*, Cornell University Press, 1979.
- 38 M. Daoud and P. G. de Gennes, *J. Phys.*, 1977, **38**, 85–93.
- 39 A. Y. Grosberg, I. Y. Erkhimovitch and E. I. Shakhnovitch, *Biopolymers*, 1982, **21**, 2413–2432.
- 40 P. G. de Gennes, *J. Phys., Lett.*, 1975, **36**, L55–L57.
- 41 J. S. Kim, V. Backman and I. Szleifer, *Phys. Rev. Lett.*, 2011, **106**, 168102.
- 42 H. Kang, P. A. Pincus, C. Hyeon and D. Thirumalai, arXiv:1409.5663v1 [cond-mat.soft].
- 43 N. H. Yazdi, C. C. Guet, R. C. Johnson and J. F. Marko, *Mol. Microbiol.*, 2012, **86**, 1318–1333.
- 44 J. K. Fisher, A. Bourniquel, G. Witz, B. Weiner, M. Prentiss and N. Kleckner, *Cell*, 2013, **153**, 882–895.
- 45 G. Zhang and C. Wu, *Phys. Rev. Lett.*, 2001, **86**, 822–825.
- 46 D. Mukherji, C. M. Marques and K. Kremer, *Nat. Commun.*, 2014, **5**, 4882.
- 47 L. E. Reichl, *A Modern Course in Statistical Physics*, John Wiley & Sons, 2nd edn, 1998.
- 48 S. Jun, D. Thirumalai and B. Y. Ha, *Phys. Rev. Lett.*, 2008, **101**, 138101.
- 49 See for instance K. A. Dill, *et al.*, *Protein Sci.*, 1995, **4**, 561–602.
- 50 W. M. Gelbart, R. F. Bruinsma, P. A. Pincus and V. A. Parsegian, *Phys. Today*, 2000, **53**, 38–44.
- 51 J. Shin, A. G. Cherstvy and R. Metzler, *New J. Phys.*, 2014, **16**, 053047.
- 52 Y. Jung, private communication, 2014.